Progress in Natural Science: Materials International 36 (2026) 195–204

HOSTED BY

Contents lists available at ScienceDirect

Progress in Natural Science: Materials International

journal homepage: www.elsevier.com/locate/pnsmi

Fast-fired and fine-grained pyrochlore dielectrics for optimized energy storage performance

Sang-il Yoon[a,c,1], Hyunseung Kim[a,b,1], Changyeon Baek[d,1], Seung Yong Lee[e], Tiandong Zhang[f], Gyoung-Ja Lee[d], Min-Ku Lee[d,*], Do Kyung Kim[e,g,**], Chang Kyu Jeong[a,b,c,***]

[a] Division of Advanced Materials Engineering, Jeonbuk National University, Jeonju, Jeonbuk, 54896, Republic of Korea
[b] Department of Energy Storage/Conversion Engineering of Graduate School (BK21 FOUR) & Hydrogen and Fuel Cell Research Center, Jeonbuk National University, Jeonju, Jeonbuk, 54896, Republic of Korea
[c] Department of JBNU-KIST Industry-Academia Convergence Research, Jeonbuk National University, Jeonju, Jeonbuk, 54896, Republic of Korea
[d] Nuclear System Integrity Sensing and Diagnosis Research Division, Korea Atomic Energy Research Institute (KAERI), Daejeon, 34057, Republic of Korea
[e] Department of Materials Science and Engineering, Korea Advanced Institute of Science and Technology (KAIST), Daejeon, 34141, Republic of Korea
[f] School of Electrical and Electronic Engineering, Harbin University of Science and Technology, Harbin, 150080, China
[g] School of Mechanical & Manufacturing Engineering, University of New South Wales (UNSW), Sydney, NSW, 2052, Australia

ARTICLE INFO

Keywords:
Pyrochlore ceramics
Fast firing
Dielectric property
Energy storage
Microstructure

ABSTRACT

In this study, the Fast Firing (Rapid Thermal Sintering, FF) process was applied to systematically analyze the microstructural, dielectric, and electrical properties of $(Bi_{1.5}Zn_{0.5})(Zn_{0.5}Nb_{1.5})O_7$ (BZN) ceramics. Through rapid heating, the target sintering temperature was reached within several minutes, effectively suppressing excessive grain coarsening and Bismuth (Bi) volatilization that commonly occur in conventional sintering (CS). As a result, BZN ceramics fabricated by the FF process exhibited a uniform fine-grained microstructure with grain sizes of 1–3 μm, relative densities above 94 %, dielectric constants (ε_r) of 145–155, dielectric losses (tan δ) below 0.005, and breakdown strengths (BDS) exceeding 400 kV/cm. Energy-storage performance analysis revealed that the FF samples achieved stable energy densities of 1.25–1.37 J/cm^3 and efficiencies of 75–85 %, which are attributed to enhanced BDS induced by the fine-grained microstructure. Frequency- and temperature-dependent measurements also demonstrated excellent thermal stability, maintaining tan $\delta < 0.005$ and dielectric variation within 3 % from room temperature up to 300 °C. In addition, the FF process shortened the sintering time by more than 70 % and reduced energy consumption, offering significant advantages in processing efficiency. These results demonstrate that the FF method provides an effective fabrication strategy for achieving high-efficiency and high-reliability energy-storage performance in BZN-based pyrochlore ceramics and further suggests its potential extension to other lead-free high-permittivity dielectric systems.

1. Introduction

With the rapid increase in demand and interest in high-power electronic devices, the development of various energy-storage media has become increasingly important [1–4]. Currently, the representative energy-storage systems are categorized into batteries [5–8] and capacitors [9–12]. A battery stores and releases energy by converting chemical energy into electrical energy; while it possesses a high energy density, it suffers from slow charge–discharge rates and strong temperature dependence. In contrast, capacitors store and release energy instantaneously based on physical polarization under an electric field, providing very high-power density, fast charge–discharge response, and long lifetime. Recently, battery–capacitor hybrid systems have attracted attention by combining the long-term energy-supply capability of

* Corresponding author. Nuclear System Integrity Sensing and Diagnosis Research Division, Korea Atomic Energy Research Institute (KAERI), Daejeon, 34057, Republic of Korea.
** Corresponding author. Department of Materials Science and Engineering, Korea Advanced Institute of Science and Technology (KAIST), Daejeon, 34141, Republic of Korea.
*** Corresponding author. Division of Advanced Materials Engineering, Jeonbuk National University, Jeonju, Jeonbuk, 54896, Republic of Korea.
E-mail addresses: leeminku@kaeri.re.kr (M.-K. Lee), dkkim@kaist.ac.kr, do_kung.kim@unsw.edu.au (D.K. Kim), ckyu@jbnu.ac.kr (C.K. Jeong).
[1] These authors contributed equally to this work.

https://doi.org/10.1016/j.pnsc.2026.01.007
Received 5 November 2025; Received in revised form 6 January 2026; Accepted 19 January 2026
Available online 3 February 2026

batteries with the instantaneous power-output characteristics of capacitors [13,14]. In such systems, dielectric ceramics play a crucial role in the capacitor component. Dielectric ceramics store energy physically through polarization under an electric field without any chemical reactions, resulting in high stability and excellent performance even under high-temperature conditions [15]. Ceramics that simultaneously exhibit high dielectric constant, low dielectric losses (tan δ), and high breakdown strengths (BDS) are essential for high-power capacitors [16] and power-conversion devices [17]. Therefore, the development of high-permittivity and high-insulation dielectric materials suitable for next-generation high-power electronic components is emerging as a key technology in the automotive [18,19], communication [20], and aerospace [21] fields.

Conventional high-permittivity ceramics are primarily based on the ABO_3-type perovskite structure [22,23]. A representative material, $BaTiO_3$ (BTO), has been widely used in capacitors, multilayer ceramic capacitors (MLCC), and sensors owing to its high dielectric constant [24]. However, perovskite-structured BTO has fundamental limitations. Its strong temperature dependence (Curie temperature 120–130 °C) causes polarization collapse at elevated temperatures, which severely deteriorates energy-storage performance [25]. Moreover, its ferroelectric nature induces nonlinear polarization behavior, leading to large remnant polarization (P_r) and reduced energy efficiency [26,27]. Finally, chemical instability can result in oxygen vacancies, which in turn cause electrical-energy loss. In contrast, the $A_2B_2O_7$-type pyrochlore structure exhibits stable dielectric behavior based on its centrosymmetric crystal symmetry, low tan δ, and temperature-independent characteristics, as well as high BDS suitable for high-field energy-storage applications. Pyrochlore ceramics possess a three-dimensional network of ordered oxygen ions, providing high crystallographic stability and low dielectric nonlinearity simultaneously [26]. In other words, although pyrochlore ceramics generally exhibit lower permittivity, they offer advantages such as low loss, high insulation reliability, excellent thermal stability, and superior endurance under repeated high-temperature or high-voltage operation making them more efficient energy-storage media than perovskite ceramics under such conditions. While recent advances in high-entropy perovskite ceramics have achieved energy densities exceeding 10 J/cm^3 through multi-component compositional engineering, such systems often require complex synthesis procedures and exhibit temperature-dependent performance variations that limit thermal cycling reliability [22]. In contrast, pyrochlore-structured ceramics, despite moderate energy densities, offer inherent advantages including linear dielectric response yielding high energy conversion efficiency, centrosymmetric structure providing intrinsic phase stability, and compatibility with rapid sintering processes. This work focuses on developing BZN pyrochlore ceramics via fast firing, advancing a complementary material platform optimized for applications where thermal stability, manufacturing efficiency, and operational reliability are equally critical as energy density.

Among them, $(Bi_{1.5}Zn_{0.5})(Zn_{0.5}Nb_{1.5})O_7$ (BZN) is a representative bismuth-based, pyrochlore-type lead-free dielectric ceramic [28–31]. BZN possesses a cubic–orthorhombic dual-phase nature; the $6s^2$ lone-pair effect of Bi^{3+} ions induce strong local distortions, while the ionic substitution between Zn^{2+} and Nb^{5+} enhances dielectric stability, reduces loss, and improves BDS [31]. Reported studies have shown that partial substitution of Zinc (Zn) ions at Niobium (Nb) or Bismuth (Bi) sites stabilizes the crystal structure, leading to slim Polarization–electric field (P–E) hysteresis loops and low P_r, which directly contribute to improved energy-storage efficiency [31]. Pyrochlore's lower polarization yields linear *P-E* curves minimizing hysteresis losses and achieving 75–85 % efficiency comparable to ferroelectrics. The centrosymmetric structure with no spontaneous polarization maintains stable performance to 300 °C without ferroelectric domain reorientation, providing superior thermal reliability critical for automotive and aerospace applications.

However, Bi-based pyrochlore ceramics typically require high sintering temperatures (>1100 °C) and long dwell times during conventional sintering (CS), resulting in compositional imbalance due to Bi_2O_3 volatilization, Bi-rich secondary-phase formation at grain boundaries, and excessive grain coarsening all of which degrade dielectric and insulation properties [32,33]. Therefore, it is necessary to optimize the sintering process to enhance densification while suppressing grain growth.

Previously proposed sintering alternatives can be broadly categorized into (1) additive-assisted low-temperature sintering [34], (2) spark plasma sintering (SPS) [35], and (3) microwave sintering [36]. Additive sintering can lower the sintering temperature; however, ionic-diffusion imbalance often induces compositional distortion [34]. SPS enables densification within minutes using pulsed current, but it requires expensive high-current/high-pressure equipment and may cause graphite-die contamination and non-uniform heating [35]. Microwave sintering provides uniform bulk heating, yet temperature gradients arising from resonance inhomogeneity hinder the formation of homogeneous microstructures [36]. As an alternative to these limitations, the Fast Firing (Rapid Thermal Sintering, FF) has been proposed.

FF process can be performed under a normal air atmosphere and achieves high densification within a few minutes by rapidly reaching the target temperature and maintaining it for only a short dwell time [37]. Rapid heating significantly increases the initial sintering driving force, allowing densification to be completed within a short period while suppressing grain growth, thereby establishing an ideal kinetic window [38]. Furthermore, since no external current or vacuum equipment is required, the process is energy-efficient and industrially scalable.

According to previous reports, ceramics fabricated by the FF process exhibited reduced sintering time, lower energy consumption, relative densities above 95 %, and decreased tan δ compared with conventional methods [39]. These findings indicate that rapid thermal sintering represents more than just time reduction it serves as a key strategy enabling simultaneous optimization of ceramic performance and processing conditions.

In this study, the FF process was applied to synthesize BZN ceramics, and the effects of rapid-heating conditions on microstructure, dielectric behavior, and energy-storage properties were systematically investigated. Based on preliminary phase-formation studies, the temperature range of 1000–1100 °C was selected to balance densification kinetics with Bi_2O_3 volatilization suppression (critical vapor pressure escalates above 1050 °C). Dwell times of 5–30 min were chosen to exploit far-from-equilibrium densification mechanisms supported by recent ultrafast sintering literature, which demonstrates that rapid heating (>100 °C/min) enables densification completion within minutes while suppressing grain growth through kinetic separation of densification and coarsening phases [37,40,41]. Compared with CS, the FF process achieved target temperatures within minutes, forming a uniform fine-grained microstructure of 1–3 μm while effectively suppressing excessive grain growth and Bi volatilization. As a result, FF-BZN ceramics exhibited relative densities above 94 %, dielectric constants of 145–155, tan δ below 0.005, and BDS exceeding 400 kV/cm, with stable energy densities of 1.25–1.37 J/cm^3 and efficiencies of 75–85 %. It is noteworthy that the fine-grained structure formed under FF conditions has a more pronounced influence on improving BDS than on changing permittivity, demonstrating that enhancement of energy-storage efficiency depends primarily on microstructural homogeneity rather than on dielectric-constant increase. Therefore, this study proposes that for Bi-based pyrochlore ceramics, maximizing energy-storage performance is more effectively achieved by improving insulation reliability through microstructure refinement and densification control.

2. Experimental section

2.1. Synthesis of BZN powders

BZN ceramics were synthesized using the conventional solid-state

reaction method. High-purity Bi_2O_3 (≥99.9 %, Sigma–Aldrich), ZnO (≥99.9 %, Sigma–Aldrich), and Nb_2O_5 (≥99.9 %, Sigma–Aldrich) were used as starting raw materials. The powders were weighed according to the stoichiometric ratio and ball-milled for 24 h in ethanol (EtOH) using zirconia (ZrO_2) balls as the milling media. The resulting slurry was pan-dried to evaporate the solvent and subsequently dried overnight in an oven at 80 °C.

The dried mixture was calcined at 850 °C for 4 h. To remove the necking structure formed during calcination, the calcined powders were re-milled and subjected to the same drying procedure. The re-milled powders were then mixed with 5 wt% polyvinyl alcohol (PVA) aqueous solution as a binder and sieved through a 200-mesh screen for homogenization. The powders were uniaxially pressed into 10 mm diameter pellets, followed by cold isostatic pressing (CIP) at 200 MPa. The relative density of the green compacts was approximately 60 %.

2.2. Sintering process and furnace profiling

Sintering was performed using a rapid thermal furnace at temperatures of 1000, 1050, and 1100 °C. The hot-zone temperature profile of the furnace was measured at 10 mm intervals from the entrance to the center of the hot zone using a K-type thermocouple (Omega, USA). The temperature was held for 30 s at each position, revealing that the temperature deviation across sample positions was within ±3 °C. Measurements were carried out under the same rapid heating condition used for the BZN specimens (reaching the target temperature within 5 min). All sintering was conducted in air atmosphere, with a heating rate of approximately 100–150 $°C \cdot min^{-1}$ and a dwell time of 5–30 min, followed by natural air cooling. The relative density of the sintered specimens was determined using the Archimedes method.

2.3. Microstructural and phase analysis

Phase identification of the sintered BZN ceramics was carried out using an X-ray diffractometer (XRD, Smartlab, Rigaku) with Cu–Kα radiation (λ = 1.5406 Å). Data were collected in the 2θ range of 10°–80° with a step size of 0.02° and a scanning rate of $2° \cdot min^{-1}$. The obtained diffraction peaks were compared with the ICDD reference pattern (#14–0181) to confirm the formation of a single-phase pyrochlore structure. The microstructure was examined using a field-emission scanning electron microscope (FE-SEM, SUPRA40VP, Zeiss, Germany). The specimens were polished using SiC abrasive papers and thermally etched at 950 °C for 10 min to expose grain boundaries. The average grain size was statistically determined from more than 300 grains using ImageJ software.

2.4. Dielectric and electrical measurements

The dielectric properties were measured using an LCR meter (HP 4294 A, Agilent, USA) in the frequency range of 1 kHz–100 kHz and temperature range of room temperature–300 °C. Silver paste was applied to both surfaces of the samples as electrodes and fired at 500 °C for 30 min. P–E hysteresis loops were measured using a polarization analyzer (Poly-K, USA) under an electric field of ±200 kV/cm. The BDS was measured using a DC high-voltage source (Matsusada Precision, Japan), and the results were analyzed statistically using Weibull distribution. Cole–Cole impedance spectra were obtained using an impedance analyzer (HIOKI IM3536, Japan) over the frequency range of 1 Hz–1 MHz. These analyses were supported by the Center for University-wide Research Facilities (CURF) at Jeonbuk National University.

3. Result & discussion

In this study, the effects of the FF process on the microstructural development and densification behavior of BZN ceramics were systematically investigated. CS generally requires long dwell times to achieve sufficient densification; however, during this process, excessive grain growth and pore formation can proceed concurrently, leading to deterioration of electrical and mechanical properties [42]. These differences are schematically illustrated in Fig. 1. As shown, the traditional sintering route induces excessive grain growth due to prolonged heat treatment. However, the FF process reaches the target temperature within minutes and completes sintering in a short period, thereby effectively suppressing grain growth while achieving high relative density and low porosity. Such outcomes play a decisive role in meeting the requirements of high-permittivity and high-insulation ceramics, namely low tan δ and high BDS [43]. Fig. 2(a) presents the typical pyrochlore crystal structure of BZN ceramics. The centrosymmetric arrangement of ions at the A- and B-sites enhances dielectric stability and offers chemical robustness even at elevated temperatures. X-ray diffraction (XRD) results in Fig. 2(b) show that all major diffraction peaks match the standard $A_2B_2O_7$ pyrochlore pattern, with no detectable secondary phases such as $BiZnO_4$ or Bi_2O_3 [31], indicating complete crystallization into the target pyrochlore phase. In the pyrochlore structure, the (222) reflection ($2\theta \approx 29.1°$) and (400) reflection ($2\theta \approx 33.7°$) serve as sensitive indicators of compositional stoichiometry. The (222) peak exhibits strong structure factor contribution from A-site Bi^{3+} ions due to their high atomic scatterin, while the (400) peak is less sensitive to Bi content and serves as an internal reference. Analysis of the intensity ratio (222)/(400) reveals: FF samples maintain this ratio at 100 %, while CS samples show the ratio reduced to 80 % a 20 % reduction indicating partial Bi loss during prolonged sintering (CS: 120 min vs. FF: 30 min). Since the (222) reflection scattering intensity is dominated by Bi contributions, preferential Bi volatilization manifests as disproportionate decrease in (222) relative to (400). The preserved intensity ratio in FF samples demonstrates that the abbreviated thermal profile (<30 min dwell) effectively suppresses Bi_2O_3 evaporation despite exposure to high temperatures (1050 °C), maintaining A-site stoichiometry and ensuring phase purity. The sintering process was carried out using a rapid thermal furnace, as shown in Fig. 2(c), which was designed to secure a uniform temperature distribution within the alumina tube. Fig. 2(d) depicts the temperature gradient along the furnace length, revealing a steep rise in the 200–300 mm region and attainment of the set temperature near 500 mm. This indicates that temperature deviations depending on sample position can directly affect microstructural uniformity. Indeed, density variations were observed in early trials depending on sample placement; however, through positional optimization, the temperature difference among samples was controlled within 3 °C. These results are consistent with previous reports on rapid thermal processing of $BaTiO_3$-based ceramics, wherein rapid heating enabled energy savings while maintaining high permittivity. Moreover, studies on Bi-based pyrochlore ceramics have suggested that high-rate sintering is effective for controlling grain size and improving mechanical strength [26, 44]. The present BZN results are in line with these precedents, indicating that the FF route is optimized for producing high-efficiency, high-density ceramics.

Fig. 3 shows FE-SEM micrograph of BZN surfaces obtained under various sintering temperatures and times. In all samples, the average grain size increased gradually with increasing temperature and dwell time, while the particle size distribution remained homogeneous irrespective of the thermal profile. Notably, FF samples exhibited a uniform fine-grained microstructure with grain sizes of 1–3 μm, and no abnormal grain growth was observed. However, in the CS route, prolonged heat treatment (≥120 min) resulted in grains exceeding 5 μm and an increased porosity. This is attributed to accelerated mass transport and enhanced grain-boundary coalescence under extended high-temperature exposure [45]. During FF, the high sintering driving force acts rapidly in the initial stage due to steep heating, while the short dwell time suppresses grain-boundary migration, thereby yielding smaller grains alongside higher density. This behavior conforms to stage-wise grain-growth models, implying that diffusion-limited mechanisms are predominant under rapid thermal treatment. Rapid heating

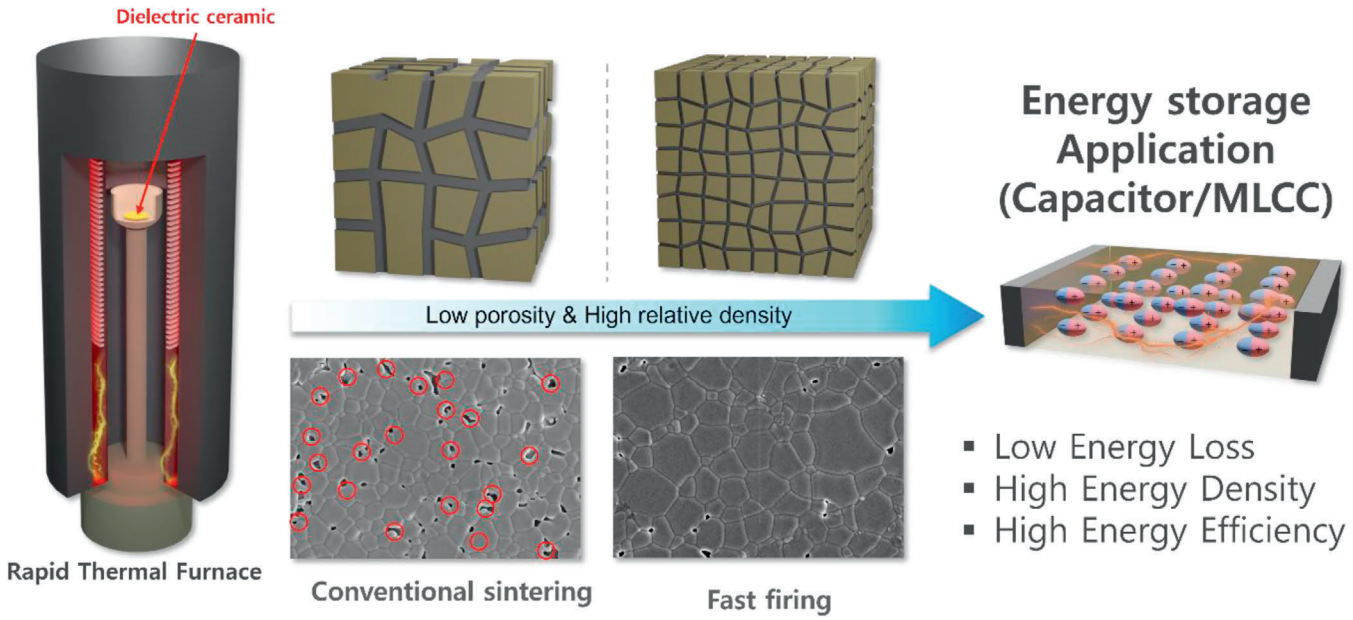

Fig. 1. Schematic representation of the relationship between rapid sintering, microstructure modification, and energy storage performance in ceramics.

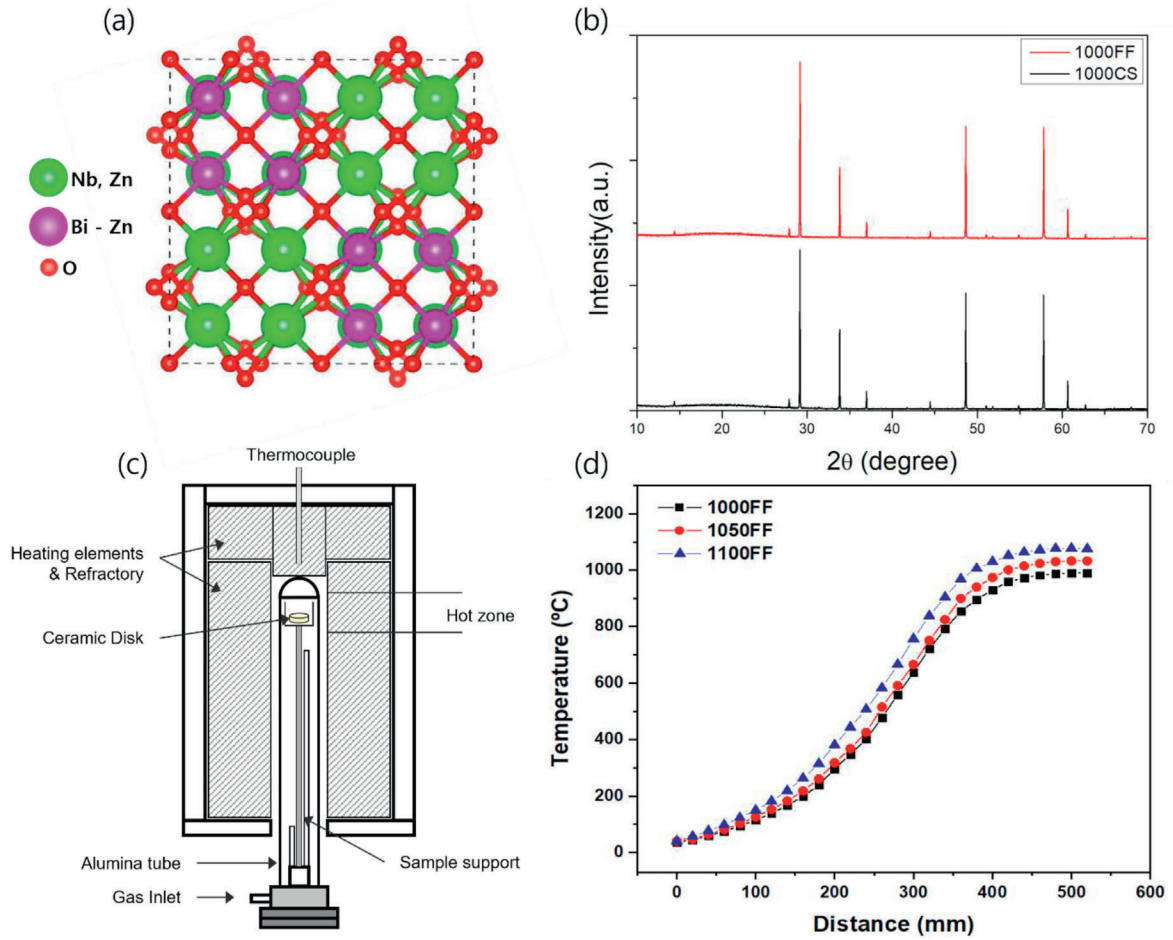

Fig. 2. (a) Crystal structure of $(Bi_{1.5}Zn_{0.5})(Zn_{0.5}Nb_{1.5})O_7$ (BZN) with a typical pyrochlore framework, (b) X-ray diffraction (XRD) pattern confirming the formation of pyrochlore structure, (c) Photograph of the rapid sintering furnace setup, showing sample arrangement and chamber design, (d) Temperature profile of the hot zone as a function of distance from the center, illustrating spatial thermal gradients within the sintering furnace.

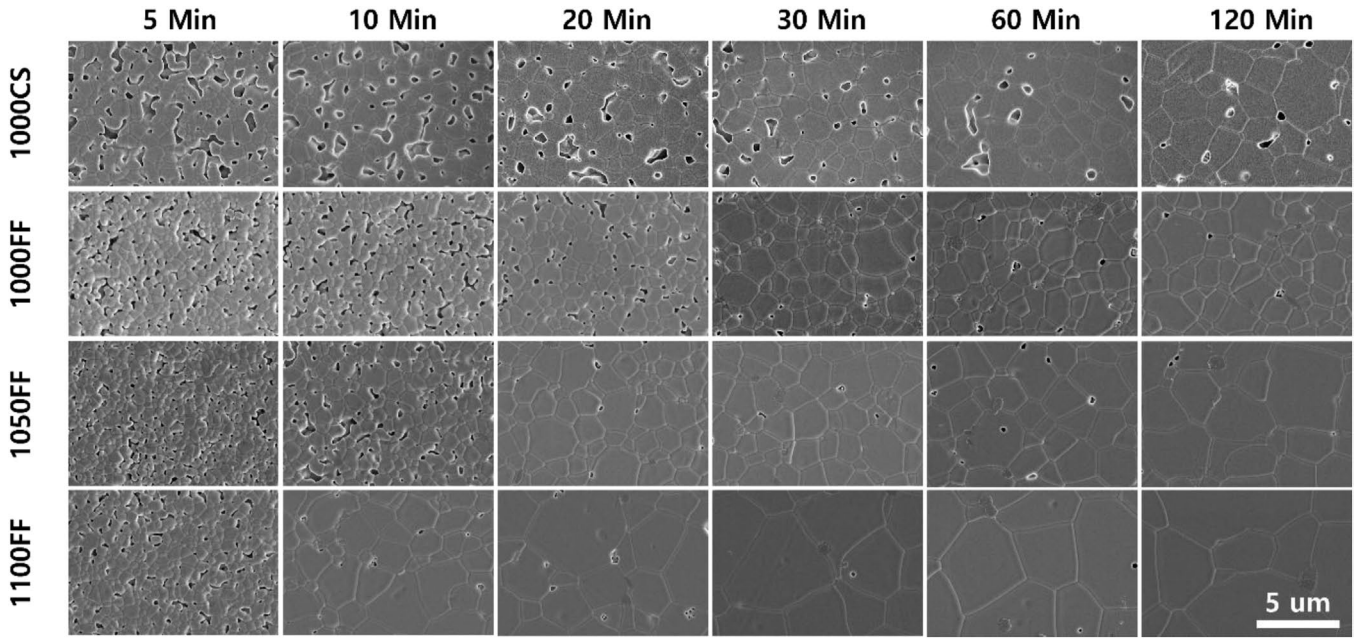

Fig. 3. Polished surface SEM micrographs of BZN bulk ceramics sintered under various conditions.

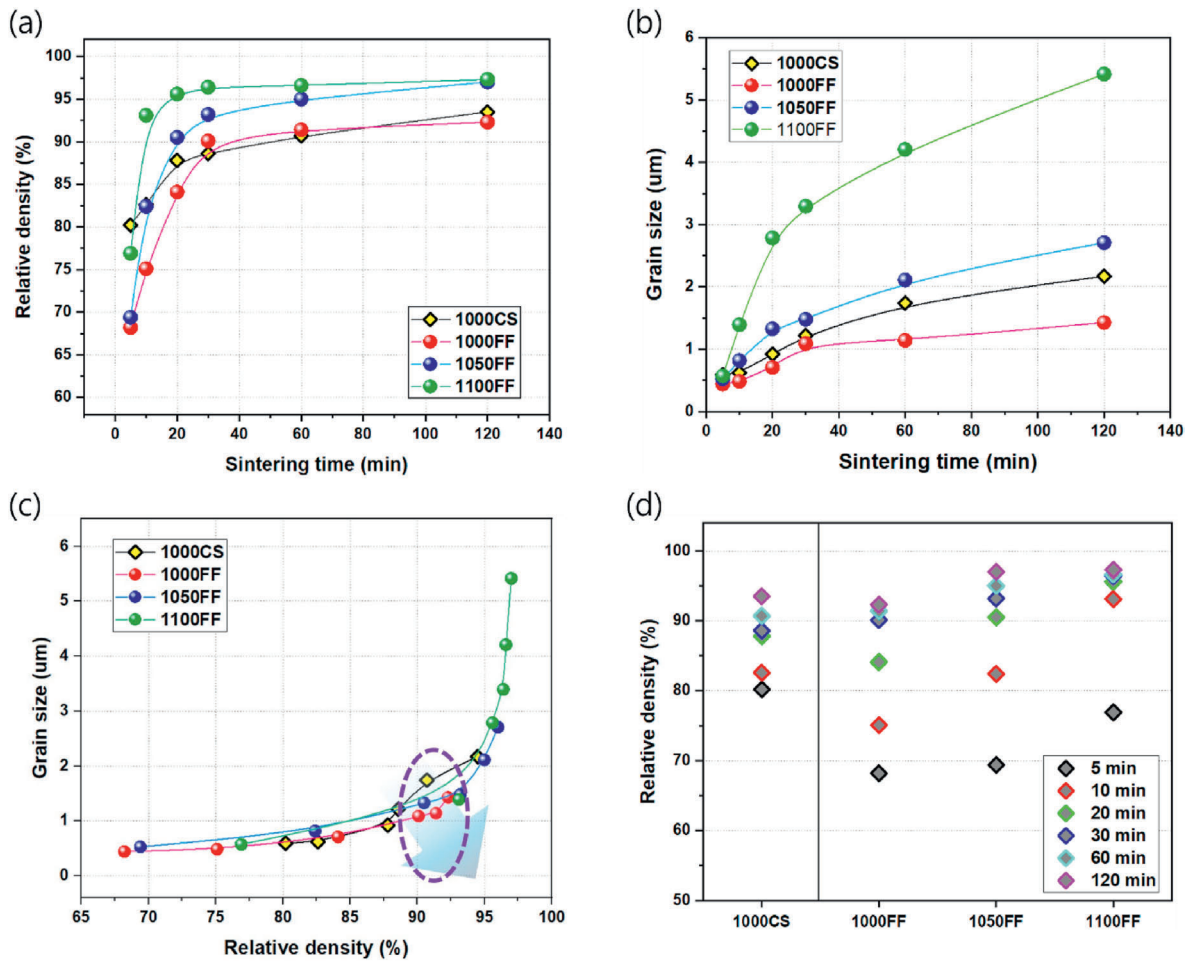

Fig. 4. (a) Relative density of BZN bulk ceramics as a function of sintering time under various sintering conditions. (b) Average grain size variation with respect to sintering time. (c) Correlation plot between relative density and average grain size, indicating a trade-off between densification and grain growth. (d) Comparative bar chart of relative densities for samples sintered at different durations, highlighting the influence of dwell time on densification behavior.

generates non-equilibrium vacancy supersaturation, creating steep chemical potential gradients that accelerate grain boundary diffusion. FF's brief dwell time suppresses extensive grain boundary migration. Experimental validation: FF achieved >94 % density in 30–60 min (vs. >120 min for CS), and despite higher peak temperature, FF grain size was 2–3 × smaller (1–3 μm vs. 5–7 μm), demonstrating that time-at-temperature dominates grain growth kinetics. As a result, at identical peak temperatures, FF samples exhibited approximately 20 % higher relative density than their CS counterparts. The pore analysis confirms grain size 3.69 ± 2.44 μm (1–10 μm range) and average pore diameter 0.53 ± 0.44 μm with >80 % of pores <1 μm (closed porosity). This submicron, isolated pore structure is consistent with ~4–6 % total porosity (i.e., >94 % relative density) and minimizes electric field concentration, explaining >400 kV/cm breakdown strength.

This trend is also supported by prior studies, which reported that decreasing grain size in dielectrics can enable simultaneous enhancement of BDS and reduction of tan δ [46]. Therefore, the fine-grained microstructure produced by the FF process constitutes a favorable condition for energy-storage applications. Fig. 4(a) displays the evolution of relative density with sintering method and time, while Fig. 4(b) shows the corresponding average grain sizes. Most densification proceeded rapidly within the first 60 min, and FF conditions achieved high densities (>94 %) even with short dwell times. Fig. 4(c) correlates relative density with grain size: at a similar density level (≈90 %), FF samples maintained much smaller grains than CS samples, highlighting that FF provides a superior balance in the density–grain-size trade-off. FF at 1050 °C/30 min yields 2–3 μm grains at >94 % density; CS at 1000 °C/120 min yields 5–7 μm at ~92 % density. Despite FF's higher temperature, grain size reduction proves time-at-temperature dominates grain growth kinetics over absolute temperature. Fig. 4(d) further shows that FF samples reached relative densities ≥94 % at 30–60 min, representing an ideal microstructure for high-permittivity ceramics. These findings are consistent with prior rapid-sintering studies on ceramics, where FF reduced total sintering time by more than 50 % while maintaining relative densities >95 % and low tan δ [41]. From a thermodynamic standpoint, FF optimizes the balance between diffusion driving force and grain-boundary resistance, enabling formation of a high-density microstructure within a short time.

The dielectric properties of BZN ceramics fabricated by CS and FF were evaluated in terms of permittivity and tan δ as functions of temperature and frequency, and the results are summarized in Fig. 5. Fig. 5 (a) shows that the CS-1000 (Conventional sintering at 1000 °C) sample exhibits dielectric constant ≈ 155 and tan δ ≈ 0.015 at room temperature. In contrast, Fig. 5(b–d) show that FF samples sintered at 1000–1050 °C exhibit dielectric constant in the range of 145–155 and tan δ of 0.005–0.02. All values are within the typical range for BZN pyrochlore ceramics reported in the literature, which is attributed to the stable polarization response of the pyrochlore structure. Low tanδ <0.005 and smooth temperature-dependent behavior confirm secondary phases <1 wt%, supporting XRD-indicated phase purity despite detection limits.

At room temperature, the CS sample shows slightly higher dielectric constant, which is ascribed to its larger grain size yielding a greater effective polarization volume. Generally, increasing grain size can enhance permittivity but often at the expense of insulation reliability, reflecting a trade-off. By contrast, FF samples simultaneously maintain relatively high dielectric constant and low tan δ despite smaller average grains, which can be attributed to suppression of leakage current via increased grain-boundary resistance and to reduced internal porosity arising from a dense microstructure [47].

Regarding temperature dependence, all FF samples maintained dielectric variation within 3 % and exhibited almost no increase in tan δ up to 300 °C, evidencing markedly improved thermal stability. This contrasts with perovskite dielectrics, which tend to show polarization

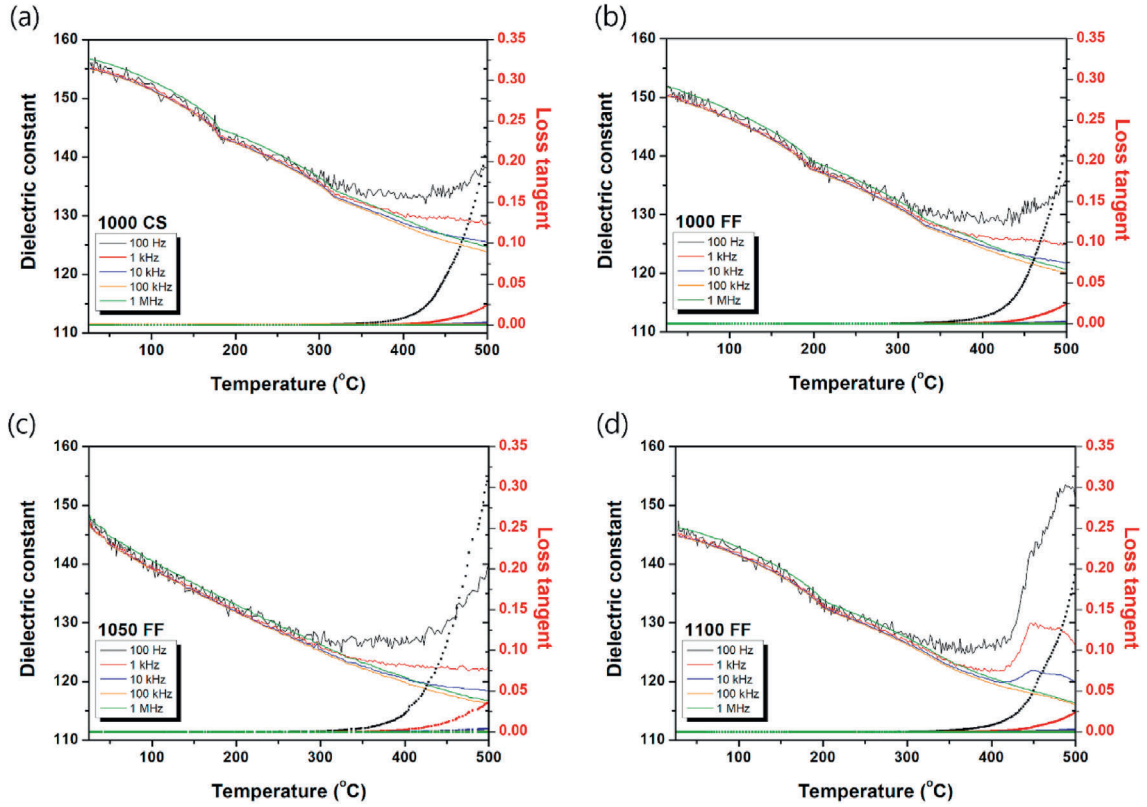

Fig. 5. Frequency and temperature-dependent dielectric constant (ε_r) and dielectric loss (tan δ) of BZN bulk ceramics sintered under different conditions.

relaxation at high temperatures; the enhanced stability here is attributed to the centrosymmetry and low oxygen-vacancy concentration intrinsic to the pyrochlore structure [48]. Pyrochlore maintains cubic symmetry to >1500 °C without displacive transitions. Strong BO_6 network resists thermal distortion. Centro symmetry eliminates spontaneous polarization and domain reorientation. Low oxygen vacancies prevent thermal leakage run away and high thermodynamic stability resists decomposition. These structural features collectively ensure 300 °C thermal stability. Frequency-dependent analyses further showed that FF samples maintained tan $\delta < 0.005$ even above 10 kHz. Such low-loss behavior is advantageous for high-frequency applications where power dissipation must be minimized. Among the FF specimens, the FF-1050 (Fast firing at 1050 °C) sample exhibited the lowest loss from room temperature to 300 °C, which is interpreted as an optimal balance between grain size and relative density. This tendency resembles results reported for pyrochlore composites processed by rapid sintering, wherein high-rate

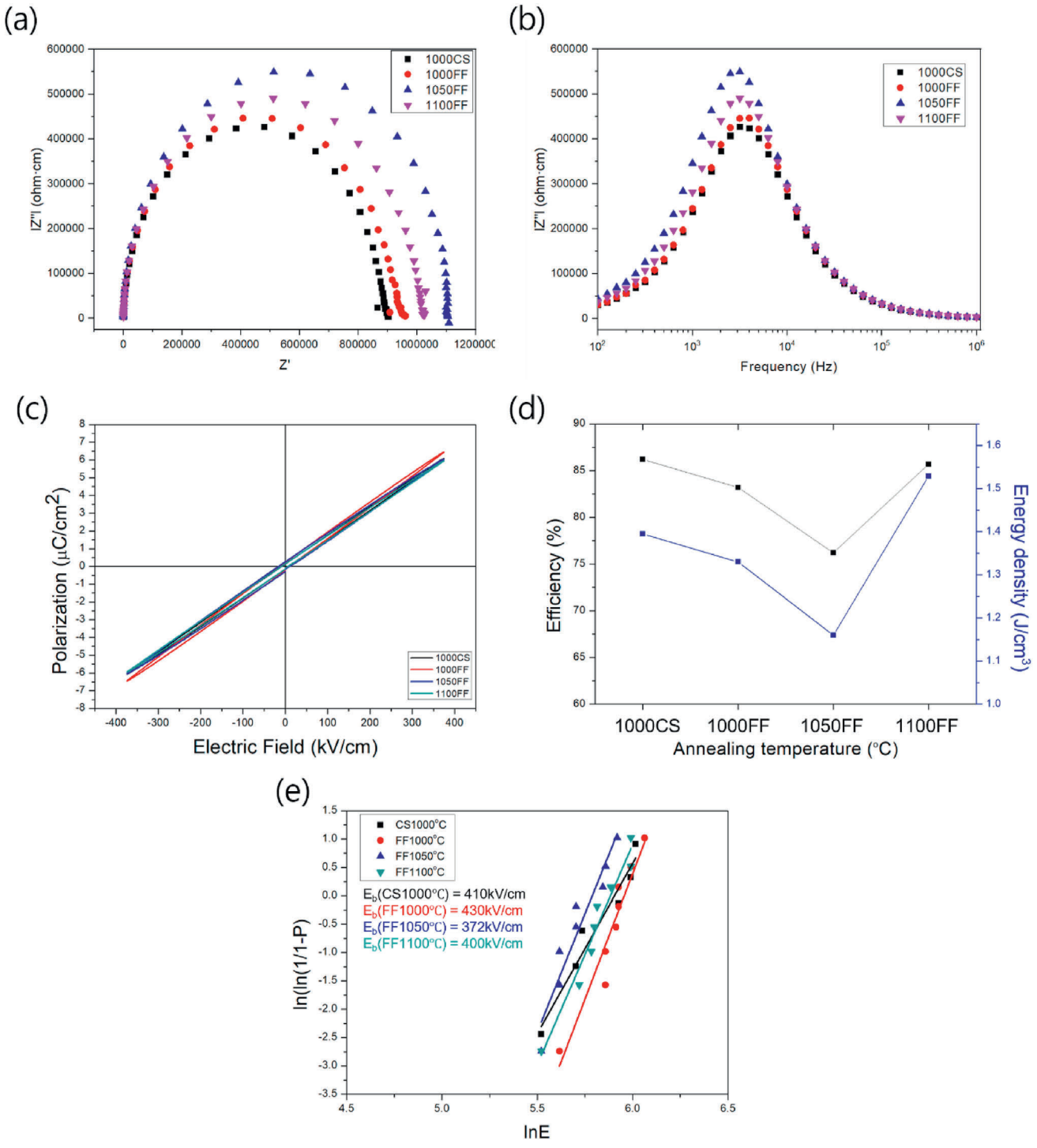

Fig. 6. (a) Cole–Cole plots of BZN bulk ceramics sintered under different conditions, showing impedance response and grain/boundary contributions. (b) Frequency-dependent impedance spectra, indicating resistive and capacitive behavior across the measured range. (c) Polarization–electric field (P–E) hysteresis loops. (d) Calculated energy density and energy efficiency based on P–E loops, highlighting the influence of sintering conditions on energy storage performance. (e) Weibull distribution analysis of breakdown strength for BZN ceramics under varying sintering conditions, including linear fitting curves to evaluate dielectric reliability.

heating suppressed grain-boundary polarization and enabled stable dielectric behavior with tan δ < 0.006 [49]. Accordingly, BZN ceramics fabricated via FF exhibited less than half the tan δ of CS samples under the same temperature conditions and showed markedly alleviated temperature and frequency dependences. These results indicate that FF can simultaneously realize microstructural uniformity and enhanced grain-boundary resistance, thereby ensuring stable dielectric response even under high-temperature and high-frequency environments.

The electrical and energy-storage behaviors of BZN ceramics were further analyzed using Cole–Cole impedance spectra, P–E hysteresis loops, and Weibull statistics for BDS. Fig. 6(a) presents Cole–Cole plots, separating the impedance contributions from grains and grain boundaries. Under identical thermal histories, FF samples exhibit larger arc radii than CS samples, implying higher resistivity and improved insulation. This is interpreted as a consequence of the fine-grained microstructure produced by FF, which partitions current pathways and suppresses electronic conduction and leakage. FF-1050 and FF-1100 (Fast firing at 1100 °C), in particular, show higher insulation due to reduced porosity and increased relative density. The Cole-Cole impedance plots reveal markedly larger impedance arcs (higher resistance) for FF samples, indicating that FF's increased grain boundary density creates longer effective percolation paths for charge carriers, elevating bulk resistivity. The space-charge polarization comprises ~30–35 % of total polarization in CS samples but only ~10–15 % in FF samples. This threefold reduction directly results from elevated grain boundary resistance and reduced trap state densities. This polarization mechanism redistribution explains why FF samples produce slim P-E hysteresis loops with superior energy conversion efficiency (75–85 % vs. ~70 % in CS). Fig. 6 (b) shows frequency-dependent impedance. All specimens display high resistance in the low-frequency region (10^2–10^3 Hz), followed by a gradual decrease around 10^3–10^4 Hz. This behavior can be interpreted as high-frequency charge transport responding rapidly by effectively bypassing grain-boundary resistance, while in the low-frequency domain larger space-charge accumulation contributes to suppressing energy loss [50]. Therefore, FF simultaneously satisfies two seemingly conflicting requirements: loss suppression at low frequencies and fast response at high frequencies. Fig. 6(c) shows P–E hysteresis loops for each sample. All BZN ceramics exhibit the characteristic weakly nonlinear behavior of pyrochlore dielectrics, with slim loops and low Pr, indicative of largely reversible polarization suitable for energy-storage dielectrics. The observed slim polarization-electric field (P-E) hysteresis loops can be understood through analysis of different polarization mechanism contributions. Total polarization in BZN ceramics comprises four additive contributions with distinct characteristics. Electronic polarization (~12–15 %) arises from electron cloud distortion with response time ~10^{-15} s, making it frequency-independent and unaffected by sintering microstructure as it represents intrinsic atomic response. Ionic polarization (~50–55 %, dominant) results from relative displacement of cations and anions within the pyrochlore lattice with response time ~10^{-13} s, largely temperature-stable and reversible, contributing minimally to hysteresis. Dipolar polarization (<5 %, negligible) is virtually absent in centrosymmetric BZN pyrochlore due to lack of spontaneous polarization and ferroelectric domains, fundamentally distinguishing pyrochlore from ferroelectric perovskites. Space-charge polarization (~30–35 % in CS, ~10–15 % in FF) arises from charge carrier accumulation at grain boundaries. Rapid sintering dramatically suppresses this through elevated grain boundary resistance and reduced defect density. The three-fold reduction in space-charge contribution is the primary mechanism by which FF improves energy efficiency (from ~70 % in CS to 75–85 % in FF). The dramatic space-charge suppression results in reduced hysteresis width, lower Pr, and superior charge-discharge efficiency. FF samples show narrower loop widths and lower Pr than CS samples, reflecting minimized charge trapping and superior polarization recoverability. Based on P–E hysteresis loops (Fig. 6(d)), the CS-1000 sample achieves an energy density of 1.37 J/cm^3 with an efficiency of 85 %. The FF-1000 (Fast firing at 1000 °C) sample, while benefiting from improved insulation via microstructural control, exhibits slightly lower dielectric constant and thus shows 1.25 J/cm^3 and 82 % efficiency. The FF-1050 specimen presents relatively lower energy density but higher BDS, ensuring stable operation. These results clearly demonstrate a trade-off wherein increasing grain size can contribute to higher permittivity yet may degrade insulation reliability [51]. Weibull analysis (Fig. 6(e)) yields an average BDS of 410 kV/cm for CS-1000, while FF samples exhibit values ≥ 400 kV/cm. The low standard deviation (<5 %) across all samples confirms the process repeatability and reproducibility of FF. The enhanced BDS is attributed to the dense microstructure and uniform grain-boundary distribution realized by FF. Similar observations have been reported for Bi-based pyrochlore dielectric films, where rapid heating enabled energy densities exceeding 1.4 J/cm^3 alongside high breakdown reliability [52]. Table 1 shows FF-BZN's unique positioning: unmatched processing efficiency (<60 min), superior thermal stability (300 °C), and compositional simplicity without competing for peak energy density. This paradigm shift toward manufacturability and reliability addresses critical industrial bottlenecks in commercialization.

The present work focused particularly on the combined effects of temperature and time. Furthermore, In FF, increasing the heating rate while shortening the dwell time limits diffusion and suppresses grain growth, while relatively enhancing the densification driving force. This is because fine particles with high specific surface area rapidly neck and consolidate during the initial stage of sintering. Conversely, prolonged sintering promotes excessive grain-boundary migration and intergranular coalescence, leaving residual pores and producing heterogeneous microstructures; these effects increase tan δ and undermine insulation reliability [58]. Therefore, the FF window of 1000–1050 °C for 30–60 min is evaluated as optimal, delivering relative density >94 %, average grain size ≤2 μm, BDS >400 kV/cm, and tan δ < 0.005. Such optimization is also significant from an energy perspective: compared with CS, FF reduces total sintering time by more than 70 % and lowers energy consumption. In addition, the thermal gradients arising during rapid heating can facilitate stress relaxation at grain boundaries, aiding the formation of uniform microstructures.

As a result, FF represents more than a simple reduction in processing time; it is a strategy for simultaneous optimization of performance and processing in ceramic materials. Furthermore, comprehensive structural, dielectric, and electrical characterizations of BZN ceramics fabricated by FF were conducted. Particularly, FF yielded the following key improvements: a uniform fine-grained (1–3 μm) microstructure with minimized porosity and high relative density; low tan δ (<0.005) with stable permittivity in the 145–155 range; and electrical performance

Table 1
Comprehensive comparison of recent energy storage ceramics.

Material	Type	Method	Wrec (J/cm^3)	η (%)	BDS (kV/cm)	T-Stability	Time	Reference
FF-BZN	Pyrochlore	FF	1.25–1.37	75–85	>400	25–300 °C	<60 min	This work
High-entropy $BaTiO_3$	Perovskite	CS	10.9	93	720	−50-260 °C	>2 h	[22]
KNN-SNZ	Perovskite	CS	14	89	760	Wide	>2 h	[53]
$AgNbO_3$-based	Perovskite	CS	9.27	83.2	510	RT-stable	>4 h	[54]
BNT High-entropy	Perovskite	CS	7.57	81.8	572	Stable	>2 h	[55]
$NaNbO_3$-based	Perovskite	CS	5.41	86.7	*	25–150 °C	>2 h	[56]
$BiFeO_3$-$CaTiO_3$	Perovskite	CS	1.18	85	190	RT-190 °C	>2 h	[57]

characterized by BDS >400 kV/cm and energy efficiency of 75–85 %. In particular, FF conditions within 1000–1050 °C provided the most favorable balance between microstructure and electrical properties. The approach effectively addresses the high-temperature polarization instability and high-loss issues typically encountered in perovskite-based ceramics by exploiting the pyrochlore structure under FF processing. Future work should include precise control of heating/cooling rates to further improve microstructural uniformity, correction of thermal gradients in large-area samples, and long-term environmental reliability testing. Moreover, extending FF to other lead-free high-permittivity systems could accelerate the transition toward environmentally friendly, high-performance energy-storage ceramics.

4. Conclusion

In this study, the FF process was applied to BZN ceramics, and the sintering characteristics, microstructure, dielectric behavior, and electrical performance were systematically analyzed. By reaching the target temperature within minutes and completing sintering in a short time, the FF route suppressed excessive grain growth and Bi volatilization, delivering a uniform fine-grained microstructure (1–3 μm) and high relative density (≥94 %). This densified microstructure minimized electrical losses and enhanced dielectric breakdown characteristics, yielding BDSs >400 kV/cm superior to those of samples produced by CS. In terms of dielectric properties, FF samples exhibited stable values of dielectric constant (=145–155) and low tan δ (≤0.005), together with excellent thermal stability characterized by a dielectric variation within 3 % from room temperature up to 300 °C. Furthermore, they maintained a stable response without increased loss in the high-frequency region above 10 kHz, confirming their suitability for high-power capacitor applications. Electrical analyses showed slim P–E hysteresis loops with low Pr, energy densities of 1.25–1.37 J/cm^3, and energy efficiencies of 75–85 %. These findings demonstrate that the fine-grained microstructure contributes more to enhancing BDS than to increasing permittivity, indicating that improvements in energy-storage efficiency depend primarily on microstructural homogeneity rather than on the dielectric constant itself. The FF process also markedly shortened the overall sintering time and reduced energy consumption, thereby significantly improving manufacturing efficiency. Without the need for additional current supply, vacuum atmosphere, or sintering additives, it offers high industrial scalability, with excellent reproducibility and repeatability advantageous for mass production of ceramics. These results show that FF is more than a time-saving technique; it functions as a core manufacturing strategy that optimizes the structure–property relationships of ceramics. Therefore, the FF process achieves a balanced combination of high density, low loss, and high reliability while preserving the intrinsic stability and insulation characteristics of Bi-based pyrochlore ceramics. The FF-based synthesis system presented here provides a viable alternative to overcome the high-temperature instability and loss issues of conventional perovskite-based ceramics and is proposed as a promising fabrication technology for next-generation high-field energy-storage devices, high-power capacitors, and environmentally friendly lead-free ceramic applications.

CRediT authorship contribution statement

Sang-il Yoon: Writing – review & editing, Writing – original draft, Methodology, Investigation, Formal analysis, Data curation. **Hyunseung Kim:** Writing – review & editing, Writing – original draft, Methodology, Investigation, Formal analysis, Data curation. **Changyeon Baek:** Writing – review & editing, Writing – original draft, Validation, Methodology, Conceptualization. **Seung Yong Lee:** Resources, Formal analysis, Conceptualization. **Tiandong Zhang:** Validation, Investigation. **Gyoung-Ja Lee:** Validation, Investigation. **Min-Ku Lee:** Writing – review & editing, Writing – original draft, Validation, Supervision, Project administration, Investigation, Conceptualization. **Do Kyung Kim:** Writing – review & editing, Writing – original draft, Validation, Supervision, Project administration, Investigation, Conceptualization. **Chang Kyu Jeong:** Writing – review & editing, Writing – original draft, Validation, Supervision, Project administration, Investigation, Funding acquisition, Conceptualization.

Declaration of competing interest

The authors declare that they have no known competing financial interests or personal relationships that could have appeared to influence the work reported in this paper.

Acknowledgements

This work was supported by National University Development Project at Jeonbuk National University in 2024.

References

[1] W. Liu, X. Sun, X. Yan, Y. Gao, X. Zhang, K. Wang, Y. Ma, Review of energy storage capacitor technology, Batteries 10 (2024) 271, https://doi.org/10.3390/batteries10080271.
[2] G.G. Njema, R.B.O. Ouma, J.K. Kibet, A review on the recent advances in battery development and energy storage technologies, J. Renew. Energy 2024 (2024) 1–35, https://doi.org/10.1155/2024/2329261.
[3] M. Arun, S. Samal, D. Barik, S.S.R. Chandran, K. Tudu, S. Praveenkumar, Integration of energy storage systems and grid modernization for reliable urban power management toward future energy sustainability, J. Energy Storage 131 (2025) 115830, https://doi.org/10.1016/j.est.2025.115830.
[4] M. Domínguez, A. Fernández-Cardador, A. Fernández-Rodríguez, A.P. Cucala, R. R. Pecharromán, P. Urosa Sánchez, I. Vadillo Cortázar, Review on the use of energy storage systems in railway applications, Renew. Sustain. Energy Rev. 207 (2025) 114904, https://doi.org/10.1016/j.rser.2024.114904.
[5] O. Demirci, S. Taskin, E. Schaltz, B. Acar Demirci, Review of battery state estimation methods for electric vehicles - part I: SOC estimation, J. Energy Storage 87 (2024) 111435, https://doi.org/10.1016/j.est.2024.111435.
[6] S. Nyamathulla, C. Dhanamjayulu, A review of battery energy storage systems and advanced battery management system for different applications: challenges and recommendations, J. Energy Storage 86 (2024) 111179, https://doi.org/10.1016/j.est.2024.111179.
[7] M.M. Hasan, R. Haque, M.I. Jahirul, M.G. Rasul, I.M.R. Fattah, N.M.S. Hassan, M. Mofijur, Advancing energy storage: the future trajectory of lithium-ion battery technologies, J. Energy Storage 120 (2025) 116511, https://doi.org/10.1016/j.est.2025.116511.
[8] M. Amer, J. Masri, A. Dababat, U. Sajjad, K. Hamid, Electric vehicles: battery technologies, charging standards, AI communications, challenges, and future directions, Energy Convers. Manag. X 24 (2024) 100751, https://doi.org/10.1016/j.ecmx.2024.100751.
[9] S. Chen, Y. Ding, H. Mu, W. Tian, X. Deng, R. Gao, W. Cai, C. Fu, Research progress on multilayer ceramic capacitors for energy storage: review, J. Mater. Sci. Mater. Electron. 36 (2025) 77, https://doi.org/10.1007/s10854-024-14004-2.
[10] D. Li, Z. Liu, W. Zhao, Y. Guo, Z. Wang, D. Xu, H. Huang, L.-X. Pang, T. Zhou, W.-F. Liu, D. Zhou, Global-optimized energy storage performance in multilayer ferroelectric ceramic capacitors, Nat. Commun. 16 (2025) 188, https://doi.org/10.1038/s41467-024-55491-5.
[11] H. Choi, S. Pattipaka, Y.H. Son, Y.M. Bae, J.H. Park, C.K. Jeong, H.E. Lee, S.-D. Kim, J. Ryu, G.-T. Hwang, Improved energy storage density and efficiency of Nd and Mn Co-Doped Ba0.7Sr0.3TiO3 ceramic capacitors via defect dipole engineering, Materials (Basel) 16 (2023) 6753, https://doi.org/10.3390/ma16206753.
[12] Z. Zhu, Y. Bu, C. Gu, X. Wang, Advances in advanced ceramic super pseudocapacitors: principles, techniques and applications, J. Eur. Ceram. Soc. 45 (2025) 117423, https://doi.org/10.1016/j.jeurceramsoc.2025.117423.
[13] Y. Li, Y. Liu, Y. Chen, T. Liu, X. Liu, S. Ni, J. Ru, F. Meng, M. Li, Z. Cao, A battery–capacitor hybrid yarn device with excellent flexibility and high electrochemical performance, J. Mater. Chem. A 13 (2025) 12374–12382, https://doi.org/10.1039/D5TA00013K.
[14] Y. Bai, B. Cai, L. Wang, Y. Gao, X. Li, X. Yang, W. Lü, Aqueous hybrid iron-ion battery capacitors with ultra-long cycle life, Chem. Eng. J. 487 (2024) 150586, https://doi.org/10.1016/j.cej.2024.150586.
[15] M. Zhang, J. Zeng, Y. Chen, S. Lan, Y. Song, Y. Lin, Microstructure control on optimizing energy storage performance for dielectric ceramic, Rev. Mater. Res. 1 (2025) 100006, https://doi.org/10.1016/j.revmat.2025.100006.
[16] B. Zheng, Y. Lin, H. Yang, H. Jing, H. Nan, Y. Wang, F. Yao, M. Wang, Q. Yuan, A broad-high temperature ceramic capacitor with local polymorphic heterogeneous structures, Adv. Sci. 12 (2025), https://doi.org/10.1002/advs.202409814.
[17] Z. Dong, S. Zhang, L. Zhou, Flattened power converter design with improved thermal performance for high-power-density energy conversion, Energies 18 (2025) 3416, https://doi.org/10.3390/en18133416.

[18] O.A. AlKawak, J.R.R. Kumar, S.S. Daniel, C.V.K. Reddy, Hybrid method based energy management of electric vehicles using battery-super capacitor energy storage, J. Energy Storage 77 (2024) 109835, https://doi.org/10.1016/j.est.2023.109835.
[19] A. Alvarez-Diazcomas, A.A. Estévez-Bén, J. Rodríguez-Reséndiz, R.V. Carrillo-Serrano, J.M. Álvarez-Alvarado, A high-efficiency capacitor-based battery equalizer for electric vehicles, Sensors 23 (2023) 5009, https://doi.org/10.3390/s23115009.
[20] L. Ma, L. Jiang, J. Duan, Q. Du, K. Wei, H. Li, Enhanced microwave performance in spinel dielectric ceramics using entropy strategy for 5G/6G communication devices, Chem. Eng. J. 503 (2025) 158159, https://doi.org/10.1016/j.cej.2024.158159.
[21] L. Bai, X. Gao, Y. Li, Y. Li, G. Zhang, A deep insight into the additively manufactured ceramics for aerospace applications, ChemPhysMater (2025), https://doi.org/10.1016/j.chphma.2025.08.001.
[22] X. Kong, L. Yang, F. Meng, T. Zhang, H. Zhang, Y.-H. Lin, H. Huang, S. Zhang, J. Guo, C.-W. Nan, High-entropy engineered BaTiO3-based ceramic capacitors with greatly enhanced high-temperature energy storage performance, Nat. Commun. 16 (2025) 885, https://doi.org/10.1038/s41467-025-56195-0.
[23] R. Montecillo, R.R. Chien, S. Tsukada, C.-S. Chen, C.-S. Tu, K.-C. Feng, Excellent capacitive energy storage in bismuth ferrite-based multilayer ceramic, J. Eur. Ceram. Soc. 45 (2025) 117694, https://doi.org/10.1016/j.jeurceramsoc.2025.117694.
[24] J. Zhang, H. Hao, Q. Guo, Z. Yao, M. Cao, H. Liu, Dielectric and anti-reduction properties of BaTiO3-based ceramics for MLCC application, Ceram. Int. 49 (2023) 24941–24947, https://doi.org/10.1016/j.ceramint.2023.05.023.
[25] A.T. Apostolov, I.N. Apostolova, J.M. Wesselinowa, Enhanced piezoelectric and ferroelectric properties of ion-doped BaTiO 3, Phys. Status Solidi (2025), https://doi.org/10.1002/pssb.202500411.
[26] Y. Chen, J. Qi, M. Zhang, Z. Luo, Y.-H. Lin, Pyrochlore-based high-entropy ceramics for capacitive energy storage, J. Adv. Ceram. 11 (2022) 1179–1185, https://doi.org/10.1007/s40145-022-0613-3.
[27] J. Choi, K. Hyunseung, Y. Sang-il, C.K. Jeong, Quest for comparing direct-current (DC) and alternating-current (AC) poling effects on ferroelectric and piezoelectric materials, J. Korean Inst. Electr. Electron. Mater. Eng. 37 (2024) 563–581.
[28] X. Wang, H. Wang, X. Yao, Structures, phase transformations, and dielectric properties of pyrochlores containing bismuth, J. Am. Ceram. Soc. 80 (1997) 2745–2748, https://doi.org/10.1111/j.1151-2916.1997.tb03189.x.
[29] R.A.M. Osman, N. Masó, A.R. West, Bismuth zinc niobate pyrochlore, a relaxor-like non-ferroelectric, J. Am. Ceram. Soc. 95 (2012) 296–302, https://doi.org/10.1111/j.1551-2916.2011.04779.x.
[30] H. Du, X. Yao, Effects of Sr substitution on dielectric characteristics in Bi1.5ZnNb1.5O7 ceramics, Mater. Sci. Eng. B 99 (2003) 437–440, https://doi.org/10.1016/S0921-5107(02)00447-6.
[31] S.Y. Lee, H. Kim, C. Baek, K.-I. Park, G.-J. Lee, S.-H. Kim, J.-H. Lee, M.-K. Lee, D. K. Kim, C.K. Jeong, Yielding optimal dielectric energy storage and breakdown properties of lead-free pyrochlore ceramics by grain refinement strategies, J. Alloys Compd. 1008 (2024) 176569, https://doi.org/10.1016/j.jallcom.2024.176569.
[32] A. Mahajan, H. Zhang, J. Wu, E. Venkata Ramana, C. Yu, N.V. Tarakina, M. J. Reece, H. Yan, Effect of processing on the structures and properties of bismuth sodium titanate compounds, J. Mater. Res. 36 (2021) 1195–1205, https://doi.org/10.1557/s43578-020-00040-1.
[33] Q. Xu, Y.-H. Huang, M. Chen, W. Chen, B.-H. Kim, B.-K. Ahn, Effect of bismuth deficiency on structure and electrical properties of (Na0.5Bi0.5)0.93Ba0.07TiO3 ceramics, J. Phys. Chem. Solid. 69 (2008) 1996–2003, https://doi.org/10.1016/j.jpcs.2008.02.009.
[34] D. Han, S. Uemura, C. Hiraiwa, M. Majima, T. Uda, Detrimental effect of sintering additives on conducting ceramics: Yttrium-doped barium Zirconate, ChemSusChem 11 (2018) 4102–4113, https://doi.org/10.1002/cssc.201801837.
[35] M. Stuer, P. Bowen, Z. Zhao, Spark plasma sintering of ceramics: from modeling to practice, Ceramics 3 (2020) 476–493, https://doi.org/10.3390/ceramics3040039.
[36] M. Oghbaei, O. Mirzaee, Microwave versus conventional sintering: a review of fundamentals, advantages and applications, J. Alloys Compd. 494 (2010) 175–189, https://doi.org/10.1016/j.jallcom.2010.01.068.
[37] O. Guillon, W. Rheinheimer, M. Bram, A perspective on emerging and future sintering technologies of ceramic materials, Adv. Eng. Mater. 25 (2023), https://doi.org/10.1002/adem.202201870.
[38] D. Wang, X. Wang, C. Xu, Z. Fu, J. Zhang, Densification mechanism of the ultra-fast sintering dense alumina, AIP Adv. 10 (2020), https://doi.org/10.1063/1.5119030.
[39] C.R. Bowen, J. Open, J. Fitzmaurice, S. Mahon, Fast firing of electroceramics, Ferroelectrics 228 (1999) 159–166, https://doi.org/10.1080/00150199908226133.
[40] Y. Zhu, J. Zhang, W. Li, Y. Xue, J. Yang, S. Li, Realization of superior ionic conductivity by manipulating the atomic rearrangement in Al-doped Li7La3Zr2O12, Ceram. Int. 49 (2023) 10462–10470, https://doi.org/10.1016/j.ceramint.2022.11.230.
[41] L. Fu, J. Wu, S.K.M. Sathyanath, B. Wang, K. Leifer, H. Engqvist, S. Grasso, W. Xia, Far from equilibrium ultrafast high-temperature sintering of ZrO 2 –SiO 2 nanocrystalline glass–ceramics, J. Am. Ceram. Soc. 106 (2023) 4005–4012, https://doi.org/10.1111/jace.19055.
[42] H. Palneedi, P. Sharief, S. Hong, J. Kim, M. Uzair, S. Jeon, J. Guo, Densification and grain growth in ceramics fabricated by cold sintering: a review on the effect of process parameters, J. Am. Ceram. Soc. 109 (2026), https://doi.org/10.1111/jace.70268.
[43] A. Jan, H. Liu, H. Hao, Z. Yao, M. Emmanuel, W. Pan, A. Ullah, A. Manan, A. Ullah, M. Cao, A.S. Ahmad, Enhanced dielectric breakdown strength and ultra-fast discharge performance of novel SrTiO3 based ceramics system, J. Alloys Compd. 830 (2020) 154611, https://doi.org/10.1016/j.jallcom.2020.154611.
[44] M.P. Kassarjian, B.H. Fox, J.V. Biggers, Fast firing of a lead-iron niobate dielectric ceramic, J. Am. Ceram. Soc. 68 (1985), https://doi.org/10.1111/j.1151-2916.1985.tb15219.x.
[45] Y. Nakashima, Y. Zhou, K. Hirao, T. Ohji, M. Fukushima, Effects of sintering temperature and holding time on sintering behavior, mechanical properties and thermal conductivity of silicon nitride ceramics, Ceram. Int. 51 (2025) 26757–26763, https://doi.org/10.1016/j.ceramint.2025.03.356.
[46] L. Wu, Z. Cai, C. Zhu, P. Feng, L. Li, X. Wang, Significantly enhanced dielectric breakdown strength of ferroelectric energy-storage ceramics via grain size uniformity control: phase-field simulation and experimental realization, Appl. Phys. Lett. 117 (2020), https://doi.org/10.1063/5.0027405.
[47] A. Izoulet, S. Guillemet-Fritsch, C. Estournès, J. Morel, Microstructure control to reduce leakage current of medium and high voltage ceramic varistors based on doped ZnO, J. Eur. Ceram. Soc. 34 (2014) 3707–3714, https://doi.org/10.1016/j.jeurceramsoc.2014.05.033.
[48] Y.-J. Hsiao, Y.-H. Chang, T.-H. Fang, Y.-S. Chang, Dielectric relaxation properties of perovskite-pyrochlore biphase ceramics, Appl. Phys. Lett. 87 (2005), https://doi.org/10.1063/1.2084328.
[49] A.J.M. Sales, B.M.G. Melo, S. Soreto Teixeira, S. Devesa, R.G.M. Oliveira, P.W. S. Oliveira, S.J.T. Vasconcelos, M.P.F. Graça, L.C. Costa, A.S.B. Sombra, Influence of pyrochlore phase on the dielectric properties of the bismuth niobate system, Mater. Sci. Eng. B 263 (2021) 114880, https://doi.org/10.1016/j.mseb.2020.114880.
[50] F. Rehman, J.-B. Li, M.-S. Cao, Y.-J. Zhao, M. Rizwan, H.-B. Jin, Contribution of grains and grain boundaries to dielectric relaxations and conduction of Aurivillius Bi4Ti2Fe0.5Nb0.5O12 ceramics, Ceram. Int. 41 (2015) 14652–14659, https://doi.org/10.1016/j.ceramint.2015.07.187.
[51] S.N.H. Mohd Yunus, K. Shing Fhan, B. Johar, N.M.S. Adzali, N.H. Jakfar, C. Ee Meng, E.Z. Mohd Tarmizi, Z.A. Talib, Effect of sintering temperature on dielectric and electrical properties of bio-waste derived beta-dicalcium silicate, Mater. Chem. Phys. 309 (2023) 128339, https://doi.org/10.1016/j.matchemphys.2023.128339.
[52] S.S. Won, H. Kim, J. Lee, C.K. Jeong, S.-H. Kim, A.I. Kingon, Lead-free bismuth pyrochlore-based dielectric films for ultrahigh energy storage capacitors, Mater. Today Phys. 33 (2023) 101054, https://doi.org/10.1016/j.mtphys.2023.101054.
[53] Q. Chai, Z. Liu, Z. Deng, Z. Peng, X. Chao, J. Lu, H. Huang, S. Zhang, Z. Yang, Excellent energy storage properties in lead-free ferroelectric ceramics via heterogeneous structure design, Nat. Commun. 16 (2025) 1633, https://doi.org/10.1038/s41467-025-56767-0.
[54] Y. Yang, W. Liu, X. Wang, T. Tang, L. Zhu, L. Zhao, K. Zhu, J. Wang, Phase modulation leads to ultrahigh energy storage performance in AgNbO 3 -Based ceramics and multilayer capacitors, ACS Appl. Mater. Interfaces 16 (2024) 69608–69616, https://doi.org/10.1021/acsami.4c17212.
[55] Y. Niu, F. Zhang, Z. Zhang, M. Li, J. Liu, Z.J. Wang, High-entropy composition design for achieving excellent energy storage performance in (Bi 0.5 Na 0.5) 0.94 Ba 0.06 TiO 3 -Based ceramics, ACS Appl. Electron. Mater. 7 (2025) 2629–2639, https://doi.org/10.1021/acsaelm.5c00153.
[56] K. Wei, J. Duan, X. Zhou, G. Li, D. Zhang, H. Li, Achieving ultrahigh energy storage performance for NaNbO 3 -Based lead-free antiferroelectric ceramics via the coupling of the stable antiferroelectric R phase and nanodomain engineering, ACS Appl. Mater. Interfaces 15 (2023) 48354–48364, https://doi.org/10.1021/acsami.3c09630.
[57] S. Gomasu, S. Saha, S. Ghosh, R. Bhowmik, D. Das, High energy density achieved in novel lead-free BiFeO 3 –CaTiO 3 ferroelectric ceramics for high-temperature energy storage applications, ACS Appl. Mater. Interfaces 16 (2024) 3654–3664, https://doi.org/10.1021/acsami.3c13860.
[58] W.F. Faiz Wan Ali, N.S. Abdullah, M. Kamarudin, M.F. Ain, Z.A. Ahmad, Sintering and grain growth control of high dense YIG, Ceram. Int. 42 (2016) 13996–14005, https://doi.org/10.1016/j.ceramint.2016.06.004.